ENERGY RESOLUTION AND RESPONSE ANALYSIS OF THE WEDGE 2-13 OF THE HADRON FORWARD CALORIMETER WITH ELECTRONS

by

Mehmet Deliömeroğlu

B.S., Physics, Yıldız Technical University, 2003

Submitted to the institute for Graduate Studies in
Science and Engineering in partial fulfillment of
the requirements for the degree of
Master of Science

Graduate Program in Physics

Boğazici University

2005

ACKNOWLEDGMENTS

I would like to express my grateful thanks to my thesis supervisor Professor Erhan Gulmez for his everlasting support, encouragement and concern dıring my research and for his great patience and valuable time he devoted to evaluate and read the drafts of this thesis.

I specially would like to thank Professor Metin Arik and Professor Engin Işıksal for their kindly reading and evaluating my thesis.

I would like to thank Boğazici University Research Fund (04B301) for their contribution.

ABSTRACT

ENERGY RESOLUTION AND RESPONSE ANALYSIS OF THE WEDGE 2-13 OF THE HADRON FORWARD CALORIMETER WITH ELECTRONS

CMS is one of the major detectors in the Large Hadron Collider (LHC) and it is built to check postulations of the standard model, especially, the Higgs mechanism. The HF calorimeter is part of the CMS detector to detect forward jets. The HF Forward Calorimeter is designed as a quartz fiber calorimeter (QFCAL). It is important to understand the energy resolution and response of the HF calorimeter.

In this work, the test beam data taken during the HF Test Beam 2004 period are analyzed using "*root*", *an Object Oriented Data Analysis Framework*. The energy resolutions and energy response values of the wedge 2-13 of the HF Calorimeter with electrons are determined as a function of both tower number and beam energy. The results show that the energy resolution values are reasonable for the HF Calorimeter and get better with high PMT gains. But for energy response, some deviation from the flat response is determined.

ÖZET

HADRON İLERİ KALORİMETRESİ'NİN 2-13. DİLİMİNİN ELEKTRONLAR İÇİN ENERJİ ÇÖZÜNÜRLÜĞÜ VE TEPKİSİ ÇÖZÜMLEMESİ

CMS, Büyük Hadron Çarpıştırıcısındaki önemli dedektörlerden biridir ve yapılış amacı Standart Modelin öngörülerini, özellikle Higgs mekanizmasını, araştırmaktır. HF kalorimetresi CMS dedektörünün bir parçasıdır ve ileri yöndeki jetleri inceleyecektir. HF bir kuvars telcik kalorimetresidir. HF kalorimetresinin enerji çözünürlüğünün ve tepkisinin anlaşılması önemlidir.

Bu çalışmada, 2004 HF Deneme Demeti süresinde alınan deneme demeti verileri "root", *nesne tabanlı veri çözümleme çerçevesi*, kullanılarak çözümlendi. HF kalorimetresinin 2-13. diliminin enerji çözünürlüğü ve tepkisi hem kule numarasına hem de enerjiye bağlı olarak elektronlar için yapıldı. Elde edilen sonuçlar enerji çözünürlük değerlerinin mantıklı olduğunu ve enerji çözünürlüğü değerlerinin yüksek PMT kazançları ile daha iyi olduğunu gösteriyor. Fakat enerji tepkisi için beklenen düz tepkiden bazı sapmalar tespit edildi.

TABLE OF CONTENTS

LIST OF FIGURES

LIST OF TABLES

LIST OF SYMBOLS/ABBREVIATIONS

a_0	Parameter of Least Squares Method, symbolizing y-intercept
a_1	Parameter of Least Squares Method, symbolizing the slope
c	Velocity of light in vacuum
e^-	Electron
e^+	Positron
eV	Electron-Volt
E	Energy
ΔE	Energy difference
E_0	Initial energy
E_c	Cut-off energy
E_γ	Photon energy
GeV	Giga electron-volt
n	Refractive index of medium
N_{max}	Number of particles when particle energy is equal to cut-off energy
t	Time
t_{max}	Time when particle energy is equal to cu-off energy
T	Tesla
TeV	Tera electron-volt
ν	Velocity of particle
ν_t	Threshold energy
V	Volt
Z	Atomic number
β	Ratio of the velocity particle to the velocity of light
θ	Cherenkov angle
η	Pseudorapidity
μ	Mean
σ	Uncertainty

CERN	European Organization for Nuclear Research
CMS	Compact Muon Solenoid
CSC	Cathode Strip Chambers
const.	Constant
DT	Drift Tubes
ECAL	Electromagnetic Calorimeter
EM	Electromagnetic
fluc	Fluctuation
HAD	Hadronic
HB	Hadron Barrel Calorimeter
HCAL	Hadronic Calorimeter
HE	Hadron Endcap Calorimeter
HF	Hadron Forward Calorimeter
HO	Hadron Outer Calorimeter
HV	High Voltage
instr	Instrumental
LHC	Large Hadron Collider
MSSM	Minimal Supersymmetric Standard Model
MWPC	Multiwire Proportional Chamber
PAW	Physical Analysis Workstation
PIAF	Parallel Interactive Analysis Facility
PMTs	Photomultiplier Tubes
root	An Object Oriented Data Analysis Framework
SM	Standard Model
SPS	Super Synchrotron Radiation
SUSY	Supersymmetry
sys	Systematic
UV	Ultra-violet

1. INTRODUCTION

As the energy increases in particle physics experiments, the role of calorimeters became gradually very important. The main reason for this improvement is the fact that the precision of the information provided by the calorimeters improves with the increasing energy.

Calorimeters are used to measure the energy and the position of a particle, produced in collision experiments, by absorption process. In this absorption process, the particle loses the most or all of its energy and for this reason the particle is no more available for further studies. However, there are some exceptions like muons.

Calorimeters exist in two different types as electromagnetic calorimeters and hadronic calorimeters. This separation results from the dominant interaction processes which occur during the energy loss of the incident particle. For electrons and photons the dominant process is electromagnetic interactions like Bremsstrahlung and pair production while for nucleons and mesons the dominant process is nuclear interactions like strong interactions.

Energy resolution is one of the most important characteristic of a calorimeter. Energy resolution of a calorimeter depends on the fluctuations in the energy loss processes and the technique of measuring the final products of the shower processes. The importance of these two effects in energy resolution is different in electromagnetic and hadronic calorimeters depending on their different characteristics.

In this work, I studied the energy resolution of the HF Forward calorimeter in the hadronic calorimeter system of the CMS detector. CMS is one of the major detectors in the Large Hadron Collider (LHC).

First I will describe the calorimetry in general and also briefly introduce the CMS detector in the following chapter. Then in the next chapter I will explain the test beam data I used to study the energy resolution and will give the details of the data analysis. I

will talk about my result in the chapter after that. Finally, in the last chapter, I will comment on my results.

2. CALORIMETERS

The term “calorimetry” was a method used in thermodynamics to determine the specific heat of water or other substances. There were thermally isolated boxes, called calorimeters, containing the substance of study.

In particle physics, calorimetry is a method to detect particles and measure their properties. These detection and measurement processes go through the total absorption of the particles in a block of matter which is called calorimeter.

In calorimeters, particles lose all of their energy by the absorption processes. During the absorption processes, the particle will interact with absorber material; generate secondary particles which will generate further particles, and so on, so that a shower will develop [1]. For this reason, calorimeters are also known as ‘shower counters’. Also since the particles lose all of their energy, they are no longer available for further study, and for this reason calorimeters are sometimes called as ‘destructive’ detectors.

Calorimeters [2] offer several attractive capabilities which make them important,

1. They can detect not only charged but also neutral particles by detecting the charged secondaries of them.
2. The absorption process is a statistical process, and the average number $\langle N \rangle$ of secondary particles is proportional to the energy of the incident particle. The uncertainty in the energy measurement is determined by the statistical fluctuations of N, and thus the relative energy resolution $\Delta E/E$ varies as $1/\sqrt{\langle N \rangle} \approx E^{-1/2}$
3. The different responses to hadrons, electrons and muons can be used for particle identification.
4. The signal produced can be very fast, of order of 10-100 ns, which is ideal for event selection [1].

Calorimeters can be divided into two categories as sampling calorimeters and homogenous calorimeters.

Sampling calorimeters are devices in which the energy absorption and signal generation are done by different materials, usually known as the passive and active medium, respectively. This gives a great freedom in the optimization of detectors for specific applications. The choice of a passive medium makes it possible to build compact devices, and allows optimization of, for instance, the electron/pion discrimination or position measurement. The disadvantage is that only a small fraction of the energy carried by the entering particles is deposited in the active medium that generates the signals, resulting in often considerably worse energy resolution than the homogenous one, especially for electron and photon [2].

In homogenous calorimeters, the active medium have a density that is high enough for them to be used as homogenously sensitive calorimeters. This means their entire volume is sensitive to the particles and absorbing the energy of the particles and detecting the signal produced in this process are done by the same material.

2.1. Detection Mechanism

Calorimeter signal is generated thorough various mechanisms. Some of the important ones are scintillation, Cerenkov radiation, and ionization.

2.1.1. Scintillation

Scintillation was the first physics process to be used for the generation of calorimetric signals. When a charged particle goes through matter, it loses energy. This energy can be used to bring atoms or molecules into an excited state in the matter. The excited atoms or molecules are unstable and they quickly return to the ground state. In this process, the excitation energy is released as one or more photons. When the excited energy is enough to emit visible photons, this process is called *scintillation*.

Many substances have been found to scintillate when a charged particle passes through them. Scintillators can be inorganic crystals as well as organic crystals.

Some important uses of scintillation counters are time-of-flight measurement and providing a trigger signal in an experiment.

2.1.2. Cerenkov Radiation

If a particle passes through a medium in which its velocity exceeds the velocity of light in that medium it will emit electromagnetic radiation which is known as Cerenkov radiation.

Cerenkov radiation is emitted at a characteristic angle, $\theta = \cos^{-1}(1/\ln \beta)$, with the direction of the particle, where $\beta = v/c > 1/n$, and n is the medium's index of refraction. Hence, this radiation forms a cone with half-opening angle θ.

Since the angle of emission and the intensity of radiation depend on the velocity of the particle, Cerenkov radiation can be used to determine the velocity of a charged particle.

2.1.3. Ionization

When a charged particle passes through matter, it may ionize the atoms of the matter. One or more electrons are freed by Coulomb interactions with the incident charged particle, leaving behind an ionized atom. The detection of those free charges in the matter is the fundamental process in the detection of charged particles.

2.2. Shower Developments

The characteristics of a calorimeter depend on the nature of the dominant processes responsible for energy loss. The energy loss processes for electrons and photons are the electromagnetic interactions while the energy loss process of strongly-interacting particles such as hadrons are the nuclear reactions. Since the characteristics of the electromagnetic and hadronic showers are different it is convenient to describe each separately.

2.2.1 Electromagnetic Showers

When an electron goes through matter it will radiate photons through Bremsstrahlung [3]. If the energy of the Bremsstrahlung photon is high enough it may produce an electron-positron pair or may transfer energy to electrons via Compton scattering. The pair partners will then radiate photons through Bremsstrahlung. This Bremsstrahlung and pair production process will produce an electromagnetic shower of photons, electrons and positrons. The average energy of the particles in the shower at a particular step *t*, will be

$$E(t) = E_0 / 2^t \tag{2.1}$$

where E_0 is the initial electron energy. The shower will cease when $E(t)$ becomes equal to the critical energy, ξ, at $t = t_{\max}$ where the losses due to ionization process will be comparable to that due to Bremsstrahlung process:

$$t_{\max} = t(\xi) = \ln(E_0/\xi)/\ln 2\,. \tag{2.2}$$

The maximum shower depth increases logarithmically with primary energy.

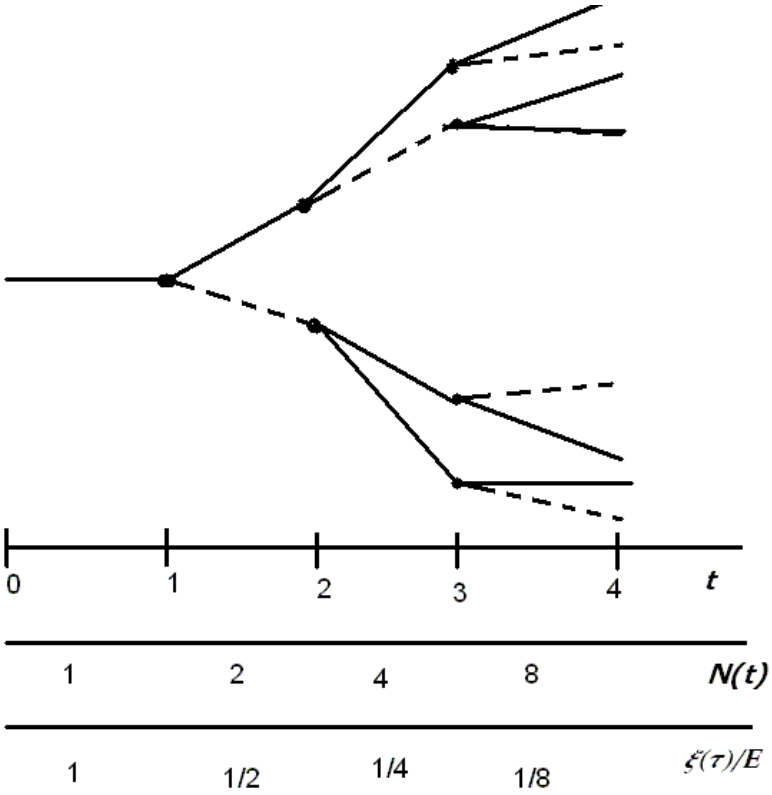

Figure 2.1 Development of an electromagnetic shower, indicating depth (t), particle number (N), fraction of the incident energy carried by each particle. Electrons and positrons are represented by straight lines while photons are represented by dashed lines.

2.2.2. Hadronic Showers

Conceptually, the energy measurement of hadronic showers is analogous to that of electromagnetic showers, but the much greater variety and complexity of the hadronic processes producing the hadronic showers makes it very complicated [2,4].

One important result of the involvement of the strong interaction is the “invisible-energy” phenomenon. In electromagnetic showers, all the energy carried by the incoming electron or photon is eventually used to ionize the absorbing medium, which is something that can be measured. However in hadronic showers a certain fraction of the dissipated energy is fundamentally undetectable. This is so because a number of the interaction processes result in neutral particles such as neutrinos and slow neutrons which escape from the calorimeter or charged particles which escape from calorimeter without

depositing their total energy. This latter effect is important for muons and also for particles back scattered in the first layers of the instrument.

When a high-energy hadron traverses a block of matter, if the hadron is charged, it will ionize the atoms of the matter. If the hadron is neutral it does not ionize the matter. For these neutral hadrons, the only option for losing their energy is nuclear reactions. This is especially true for neutrons, richly produced in hadronic shower development. For this reason, neutrons leave their kinetic energy in ways very dissimilar from those for the charged shower particles.

The particles produced in the first nuclear reaction possibly will lose their energy by ionizing the medium or induce new reactions or both, hence causing a cascade to develop. Initially, the number of cascade particles increases as a result of multiplication processes, and so does the energy deposited by the cascade particles in a slice of given thickness. A schematic picture of a hadronic shower for the first four generations is shown in Fig 2.2.

Another difference between hadronic and electromagnetic showers concerns scale of the shower development. The shower development is governed by nuclear interactions for hadronic and electromagnetic interactions for electromagnetic showers. For this reason, the scales of EM and hadronic showers are different to an amount determined by the difference between the cross sections for the EM and strong reactions.

Hadronic calorimeters are usually constructed from a stack of layers of absorbing material, such as iron, and detection devices such as scintillator or proportional counters.

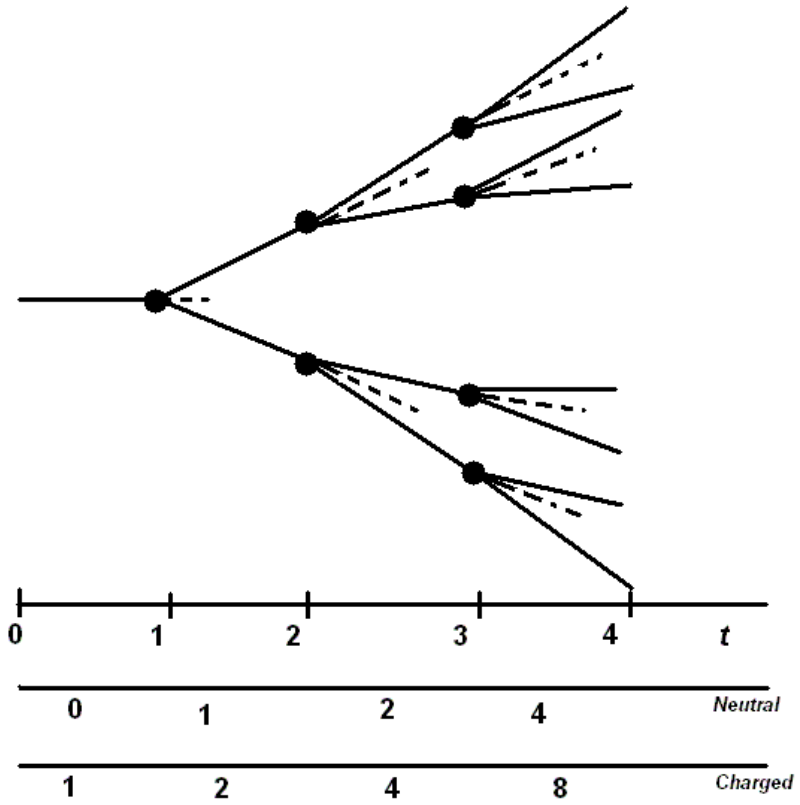

Figure 2.2 Development of a hadronic shower, indicating depth (t), neutral particle number in the shower, charged particle number in the shower. Dashed lines indicate neutral particles while straight lines represent charged particles.

2.3. Energy Resolution of Calorimeters

The energy resolution is considered the most important characteristic of a calorimeter. In particle physics experiments, the energy resolution of a calorimeter may be the factor that limits the precision with which the mass of new particles can be determined. It may limit the separation between particles with similar masses. It defines the signal-to-background ratio in event samples collected in almost every experiment that includes a calorimeter [5].

2.3.1. Energy Resolution

The precision in determining the energy of the particles is limited by two factors:

1. Fluctuations in the processes through which the energy is absorbed.

2. The technique chosen to measure the final products of the shower processes.

The fluctuations in the shower development process are unavoidable. In electromagnetic showers, they determine the ultimate limit on the achievable energy resolution. However, because of the chosen measurement techniques, the energy resolutions obtained in practice with electromagnetic calorimeters are generally worse than that.

The situations are very different for hadron calorimeters. The chosen measurement techniques have often little or no effect on the hadronic energy resolution. The effect of the intrinsic fluctuations can be partially eliminated through the design of the readout. It is possible to obtain hadronic energy resolution that is better than the limits set by the internal shower fluctuations.

The energy resolution of a calorimeter is determined by fluctuations intrinsic in the development of cascades, and by instrumental and calibration limits. The basic phenomena in showers are statistical processes, hence the intrinsic limiting factor, expressed as a fraction of total energy, improves with increasing energy as:

$$(\sigma/E)_{fluct} \propto 1/\sqrt{E} \tag{2.3}$$

Over much of the useful range of calorimeters, this term dominates energy resolution.

There are other contributions than statistics. A second component is due to instrumental effects, being rather energy-independent, its relative contribution decreases with E:

$$(\sigma/E)_{instr} \propto 1/E \tag{2.4}$$

This component may limit the low-energy performance of calorimeters.

A third component is due to calibration errors, non-uniformities and non-linearities in photomultiplier, proportional counter. The relative contribution is energy-independent:

$$(\sigma/E) = const\ . \tag{2.5}$$

This component sets the limit for the performance at very high energies.

2.3.2. Energy Resolution in EM and Hadronic Calorimeters

The two types of calorimeters, electromagnetic and hadronic, have markedly different characteristics.

2.3.2.1 Electromagnetic Calorimeters. The intrinsic limitation in resolution results from variations in the net track length of charged particles in the shower; for homogeneous shower counters

$$(\sigma/E)_{fluct} \approx 0.005/\sqrt{E} \tag{2.6}$$

In sampling calorimeters, one has to add the sampling fluctuations:

$$(\sigma/E)_{samp} \approx 0.04\sqrt{1000\Delta E/E} \tag{2.7}$$

where ΔE being the energy loss of a single charged particle in one sampling layer. There are also fluctuations arising from the Landau distribution. In practice, total energy resolution below the percent level for $E \leq 50\,\mathrm{GeV}$ can be achieved routinely in homogeneous calorimeters; the same seems more like a very tough lower limit for sampling calorimeters. At low energies and for crystal calorimeters, total energy resolutions of

$$(\sigma/E) \approx 0.025/\sqrt[4]{E} \tag{2.8}$$

have been reported.

2.3.2.2. Hadronic Calorimeters. The intrinsic limitation is due to fluctuations in the fractional energy loss accounted for by the many interaction mechanisms leaving behind non-hadronic debris (including muons and the photons and e^+/e^- from neutral pion decays) and slow neutrons, along with fast hadrons. The fluctuations in these production processes, much larger than for electromagnetic processes, are the major ingredient of the final performance of a hadron calorimeter. Intrinsic shower fluctuations are given by:

$$(\sigma/E)_{fluct} \approx 0.45/\sqrt{E} \tag{2.9}$$

for uncompensated calorimeters, and with compensation for nuclear effects

$$(\sigma/E)_{fluct} \approx 0.25/\sqrt{E}\,. \tag{2.10}$$

Compared with the intrinsic fluctuations sampling fluctuations are normally small:

$$(\sigma/E)_{samp} \approx 0.09\sqrt{1000\Delta E/E} \tag{2.11}$$

where ΔE being the energy loss by a single charged particle in one sampling layer (note that ΔE/E is a very small number). Note that these numbers refer to single hadronic particles; the σ/E for jets is typically higher by a factor of 1.3 or more.

Hadronic showers can spread over a large volume; a major source of systematic errors, therefore, is the geometric limitation of a calorimeter. The resolution figures determined by intrinsic shower and sampling fluctuations will not be reached if showers are not fully contained within the calorimeter volume. In practice some average fraction of the shower energy escapes through the sides (lateral leakage) or back (longitudinal leakage). While the corrections for longitudinal leakage are understood, and can partly be accounted for, corrections for lateral leakage need a careful inspection of the shower development and an estimate of the particle impact point.

2.4. Energy Response of Calorimeters

Response of a calorimeter is the average signal of the calorimeter divided by the energy of the particle which produced the signal. The calorimeter response depends on the signal generating mechanism and the data acquisition system. The response to the different kind of particles shows some differences.

2.4.1. Response of Homogenous Calorimeters

In homogenous calorimeters, the entire kinetic energy of electron or photon is used to generate the photons or electrons which constitute the calorimeter signal. For this reason the calorimeter should be *intrinsically linear* for E-M shower detection. This means that a 100 GeV electron should generate twice as many ion/electron pairs or scintillation photons as a 50 GeV electron.

Intrinsic linearity for E-M shower detection is an important property, not only for homogenous calorimeters but also for sampling calorimeters. However deviations from linearity may be observed, both in homogenous and sampling calorimeters. This non-

linearity may be caused by a variety of instrumental effects, *PMTs*, *showering particle density*, *light attenuation*, etc.

Because of the similarities between the energy loss mechanism of electrons and muons, the response of a homogenous calorimeter to muons and to electrons is almost equal. For example, a 100 GeV electron and a 100 GeV muon generate equal average signals.

Since only a fraction of the energy carried by hadrons and jets is used to excite the atoms or molecules of the detector medium the hadron response is smaller than E-M one for homogenous calorimeters. The response to hadrons is also energy dependent. As a result the hadronic signals from homogenous calorimeters are non-linear, in other words, the hadronic response is not constant as a function of energy.

2.4.2 Response of Sampling Calorimeters

In homogenous calorimeters, the responses to the particles which lose their energy through E-M interactions with the absorber material are the same. But for the sampling calorimeters that is not the case. For sampling calorimeters, the Z value of the absorber material is larger than the Z value of the active medium; the response to EM showers is smaller than the minimum ionizing particles (*mip*), mips are the muons with very low energy for the case. As the difference in Z value gets larger e/mip becomes smaller. In other words, the Z values of the active and passive materials of the calorimeter are the most important factors which determine the e/mip value.

The response to muons is very complicated, since the signals generated by the muons are caused by a variety of different processes. And each of these processes has its own characteristic response. For instance, the muon ionizes atoms of the absorber material and the response to this signal is the same as the *mip* response. But a high-energy muon radiates an energetic Bremsstrahlung photon; this photon develops an EM shower

and since e/mip may be different from 1.0, the response to this signal component is different from the ionization loss component.

In sampling calorimeters, the hadronic signals are non-linear, in other words the hadronic response is not constant as a function of energy. As a result, sampling calorimeters are not linear for hadronic shower detection.

3. THE CMS DETECTOR

3.1. Overview

3.1.1. The Installation

CMS [6] (The Compact Muon Solenoid) is located at Cessy in France where it is being assembled in large units in a surface hall. To simplify assembly and future maintenance the CMS yoke has been divided into 5 ring-sections and 4 disk-sections. Assembling in a surface hall, rather than the underground area, allows the construction of the magnet and detectors in parallel with the civil engineering works.

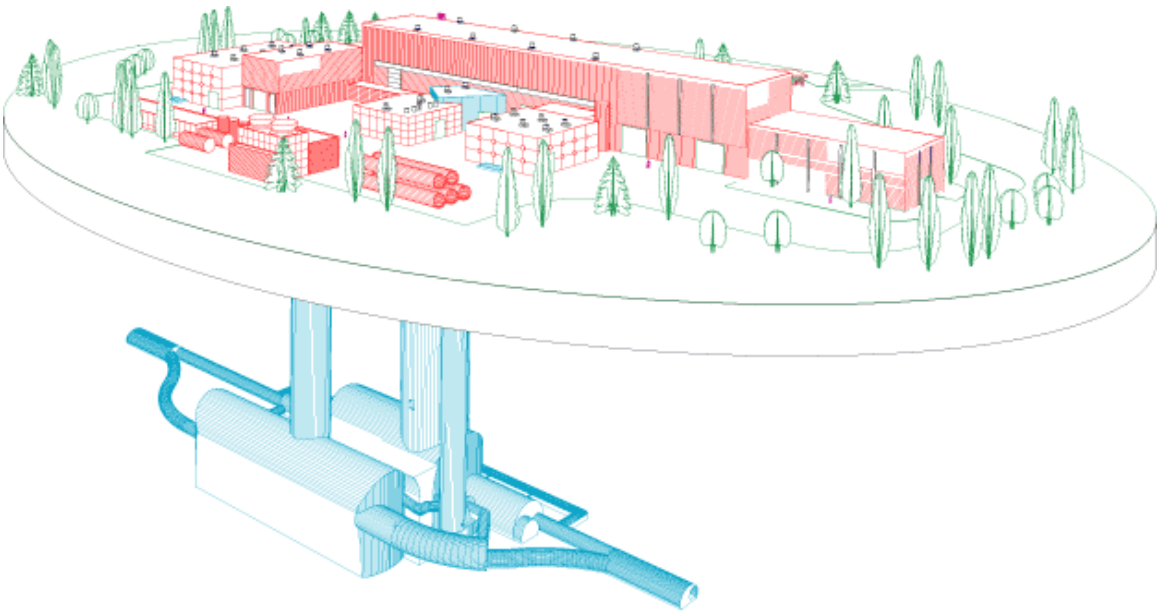

Figure 3.1 The CMS experimental area overview.

The solenoid magnet will be fully tested in the surface hall, after which complete sections of the detector will be lowered into the underground cavern.

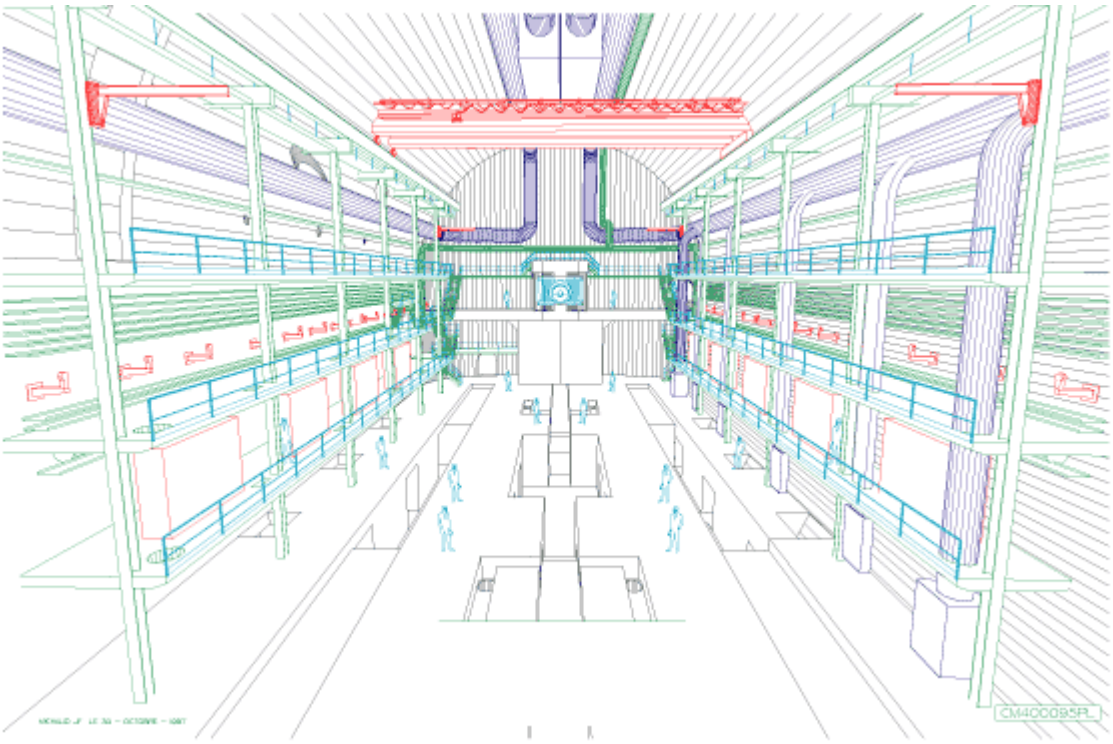

Figure 3.2 The CMS experimental hall.

3.1.2. The General Principles

CMS detector [6] is a universal physical instrument meant to detect new particles with high energy. It will be used to check assumptions of the "standard model" for particle physics, in particular, the Higgs mechanism.

The Standard Model (SM) of Particle Physics has unified the Electromagnetic interaction and the weak interaction. The intermediate bosons for e-m and weak interaction are very different: the γ is massless whereas the $W^{\pm}$ and Z^0 are quite massive (80 - 90 GeV).

In the framework of the SM particles acquire mass through their interaction with the Higgs field. This implies the existence of a new particle: the Higgs boson H^0. The theory does not predict the mass of the H^0, but it does predict its production rate and decay modes for each possible mass. CMS has been optimized to discover the Higgs in the full expected mass range 0.08 TeV < M_H < 1 TeV.

The supersymmetry (SUSY) theory which is beyond the "standard model", will be checked. The SUSY theory explains why different interactions may generate different forces. SUSY postulates a deeper relationship between matter particles (spin-1/2 or "fermions") and force carriers (integer spin or "bosons") than the Standard Model.

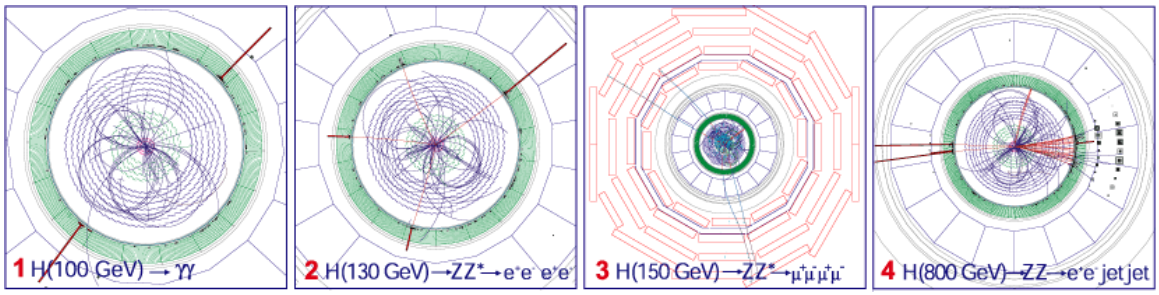

Figure 3.3 The decay signature of Higgs depending on its mass.

In SUSY, each fermion has a "superpartner" of spin-0 while each boson has a spin-1/2 superpartner. The Higgs sector is also extended to at least five Higgs bosons in the Minimal Supersymmetric Standard Model (MSSM). To this day, no superpartners have been observed: SUSY must be a broken symmetry, i.e. the superpartners must have masses different than those of their partner particles. It can also explain the presence of the "dark matter" responsible for the rapid expansion of the Universe. The detector will serve to check the hypothesis suggesting that quarks and leptons are not fundamental particles. It will also be used to look for new phenomena not studied yet.

3.1.3. The Structure

The compact muon solenoid consists of *Tracker, Electromagnetic calorimeter (ECAL), Hadronic calorimeter (HCAL), Solenoid, Magnet Yoke* and *Muon-Chambers.* The CMS detector has an over all length of 21.6m, an outer diameter of 14.6m and total weight of 12500 T. The CMS detector is shown in figure 3.4.

CMS has chosen two tracking detector technologies, each best matched to the task of satisfying the stringent resolution and granularity requirements in the high, medium and lower particle density regions.

These are silicon pixel and silicon strip detectors, arranged in concentric cylindrical volumes, at a radial distance (r) from the beamline in regions 4<r<11cm and 22<r<110cm respectively. The silicon detectors are fast, thus limiting event pileup to a single bunch crossing. The Si strip detectors cover an unprecedented area of 210m^2, consisting of ~25000 sensors with 10 million electronic channels. This large system has required the development of industrial production, assembly and testing methods.

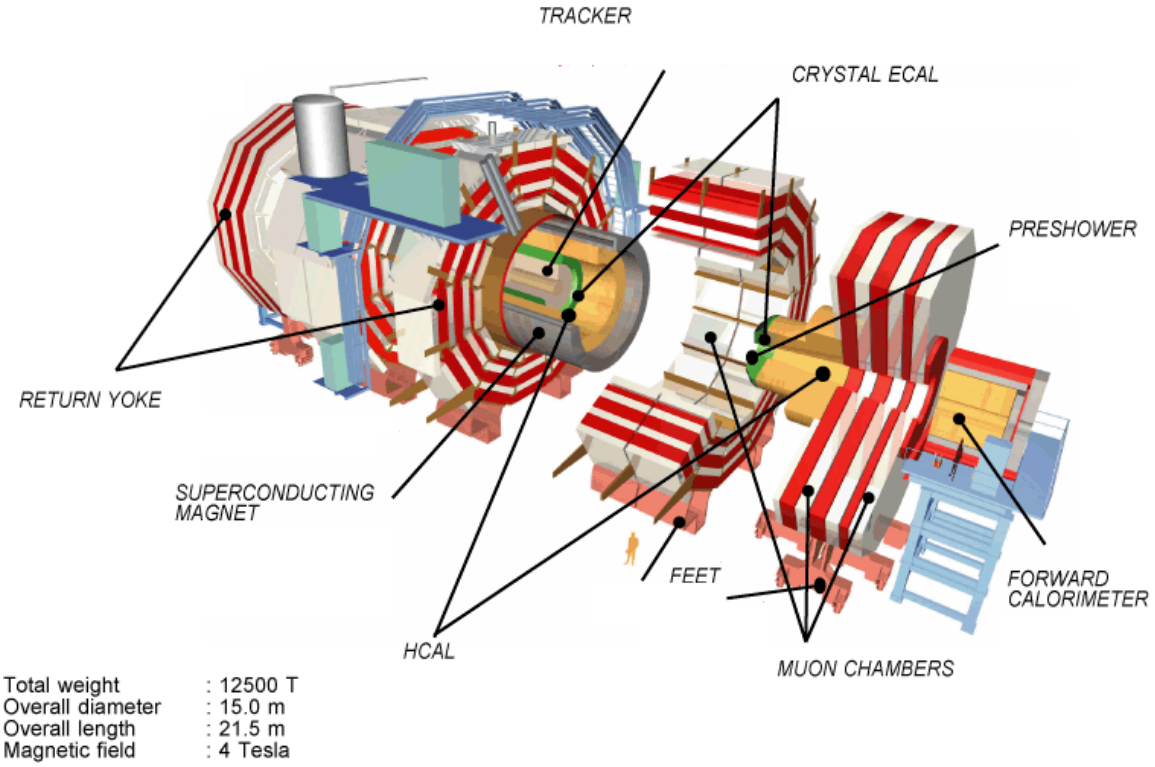

Figure 3.4. The CMS detector.

One of the principal CMS design objectives is to construct a very high performance electromagnetic calorimeter. A scintillating crystal calorimeter offers excellent performance for energy resolution since almost all of the energy of electrons and photons is deposited within the crystal volume. CMS has chosen lead tungstate crystals which have high density, a small Moliere radius and a short radiation length allowing for a very compact calorimeter system.

CMS will use three types of gaseous particle detectors for muon identification: Drift Tubes (DT) in the central barrel region, Cathode Strip Chambers (CSC) in the

endcap region and Resistive Parallel Plate Chambers (PPC) in both the barrel and endcaps.

The most important aspect of the overall detector design is the configuration and parameters of the magnetic field. The momentum measurement of charged particles in the detector is based on the bending of their trajectories. High momentum resolution is achievable either through a large bending power or through a very high precision on the spatial resolution and alignment of the detectors. For a similar bending power, the overall size of a solenoidal system is smaller than that of a toroid. The CMS design is thus based on a solenoid providing a very high (4T) magnetic field.

The CMS magnet system consists of a superconducting coil, the magnet yoke (barrel and endcap), a vacuum tank and ancillaries such as cryogenics, power supplies and process controls. It will be the largest superconducting magnet system in the world.

The magnetic yoke contains the muon chambers while the barrel parts of the hadronic calorimeter (HB), the electromagnetic calorimeter (EB), and the tracker are situated inside, and supported from the inner shell of the vacuum tank.

3.2. The Hadronic Calorimeter

The Hadronic Calorimeter (HCAL) [6] plays an essential role in the identification and measurement of quarks, gluons, and neutrinos by measuring the energy and direction of jets and missing transverse energy flow in events. Missing energy forms a crucial signature of new particles, like the supersymmetric partners of quarks and gluons. For good missing energy resolution, a hermetic calorimetry coverage to $|\eta|=5$ is required. The HCAL will also aid in the identification of electrons, photons and muons in conjunction with the tracker, electromagnetic calorimeter, and muon systems.

The HCAL has four main parts, *Hadron Barrel Calorimeter (HB), Hadron Endcap Calorimeter (HE), Hadron Outer Calorimeter (HO),* and *Hadron Forward Calorimeter (HF).* The hadron barrel (HB) and hadron endcap (HE) calorimeters are sampling

calorimeters with 50 mm thick brass absorber plates interleaved with 4 mm thick scintillator sheets.

The HB is constructed of two half-barrels each of 4.3 meter length. The HE consists of two large structures, situated at each end of the barrel detector and within the region of high magnetic field. Because the barrel part of HCAL inside the coil is not sufficiently thick to contain all the energy of high energy showers, additional scintillation layers (HOB) are placed just outside the magnet coil. The full depth of the combined HB and HOB detectors is approximately 10 absorption lengths.

The photodetectors and associated electronics will be located at the outer parts of the calorimeter. For the barrel and endcap detectors, the photosensors are hybrid photodiodes (HPDs) and for the forward detectors, conventional photomultiplier tubes are used**.**

3.3. The Hadron Forward Calorimeter

There are two hadron forward (HF) calorimeters, one located at each end of the CMS detector. The HF will be constructed as a block of steel with embedded quartz fibers, running parallel to the beam axis. HF calorimeter is a sampling calorimeter.

There are two main objectives with this detector: to improve the measurement of the missing transverse energy and to enable identification and reconstruction of very forward jets. These jets can be the distinguishing characteristic of several important physics processes or background signatures.

The HF calorimeters [7] are cylindrically symmetric around the beam line. The radius of the active part of the HF is 1.4 meters. The length, along the beam, is 1.65 m. This is satisfactory to longitudinally contain the Cerenkov signal produced by hadrons of up to 1 TeV. The central region is open to allow for the beam pipe. The HF consists of 18

wedges; each has an angle of 20 degree and includes 24 towers as shown in Figure 3.5 and Figure 3.6.

The HF is constructed such that there are two different lengths of fibers inserted into the absorber. The long fibers run the entire length of the absorber and constitute the electromagnetic section. On the other hand, the fibers shorter by 22 cm from the front face of HF constitute hadronic section.

Total HF depth is chosen to be ten interaction lengths, which is more than sufficient for the required physics performance. By increasing the absorber from eight to ten interaction lengths, a factor of two to three reduction in all particle fluxes behind the calorimeter is gained.

The main requirements for the HF are the following:

1. Phase space to be covered by the HF spans 40% of the available phase space of CMS. HF covers this region with a good hermeticity, fine transverse granularity, adequate energy resolution and a sufficient depth.

2. The HF must maintain its intended functionality even at the exceptionally high levels of radiation expected at LHC. The radiation doses of up to a Grad over ten years are anticipated in the hottest region of the HF. The choice of quartz as the active medium serves this purpose well since it can endure doses up to 30 Grad with only a few percent loss in transparency in the UV wavelengths.

3. The HF is being designed such that it integrates well with the rest of the CMS subsystems.

Figure 3.5 The HF wedges with fibers.

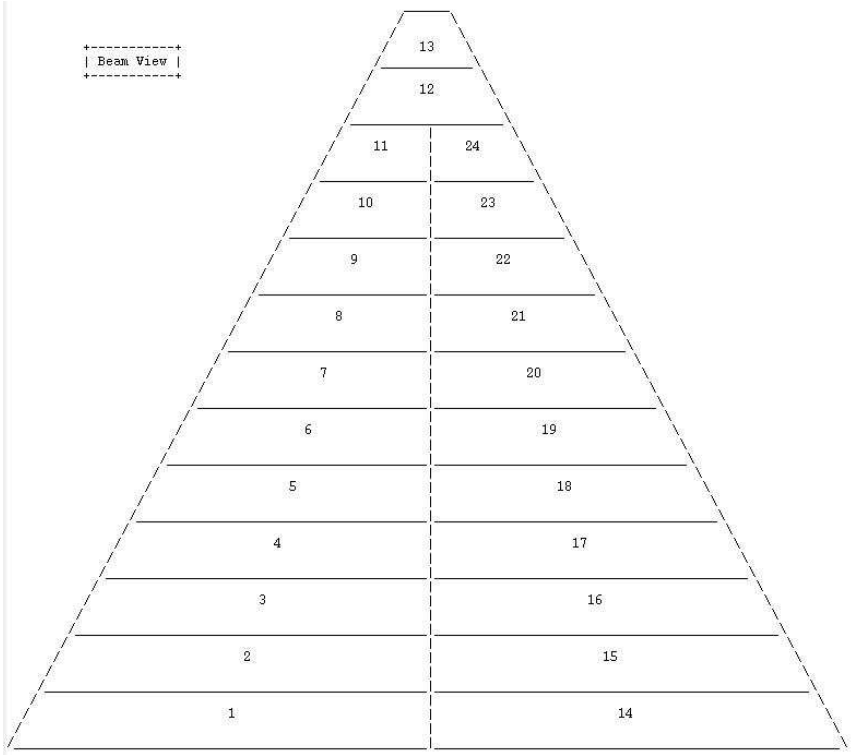

Figure 3.6 Physical map of HF.

4. DATA ANALYSIS

4.1. Data

In my analysis, I used the test beam data which were taken during the HF Test Beam 2004 period. The H2 beam line which was used during this period was in SPS (Super Proton Synchrotron) North Area located in Prevessin site, France.

In Test Beam 2004 Run, beam from H2 beam line was directed on ECAL and each part of HCAL calorimeters separately to measure their performances. Two types of data were taken; source data and beam data. The source data were taken with a 5mCi ^{60}Co source. This source was installed on a wire and run along the source channel in each tower. The source data were used to determine the PMT gains.

The beam data were taken with three different kinds of particles; electron, pion and muon at energies; 30Gev, 50GeV, 100GeV, 150GeV and 300GeV. The wedges which were used during this period were 2-1, 2-2, 2-3, 2-4, 2-6, 2-13 and 2-14.

Two sets of beam data I used in my analysis were electron beam data of wedge 2-13 (thirteenth wedge of the second HF) at HV value of 1350 V. First set consists of 4 beam runs at energies 30GeV, 50Gev, 100GeV and 150GeV for tower 2 and the second set consists of 24 beam runs at 100GeV for all Towers. These two set of data are summarized below in Table 4.1 and Table 4.2.

Table 4.1. The information about the first set of beam data.

Tower	Run #	Wedge	Particle	Events	Energy (GeV)	Tower X	Tower Y
2	22849	2-13	Electron	5000	30	2.5	2.6
2	22447	2-13	Electron	25190	50	2.5	2.5
2	23073	2-13	Electron	61020	100	2.5	2.6
2	22479	2-13	Electron	25250	150	2.5	2.6

Table 4.2. The information about the second set of beam data.

Tower	Run #	Wedge	Particle	Events	Energy (GeV)	Tower X	Tower Y
1	23070	13	Electron	60468	100	1.5	1.3
2	23073	13	Electron	61020	100	2.5	2.6
3	23075	13	Electron	60510	100	3.5	3.6
4	23076	13	Electron	61260	100	4.5	4.5
5	23077	13	Electron	60543	100	5.5	5.5
6	23078	13	Electron	60882	100	6.5	6.5
7	23079	13	Electron	60825	100	7.5	7.5
8	23080	13	Electron	60522	100	8.5	8.4
9	23081	13	Electron	61107	100	9.4	9.4
10	23082	13	Electron	60876	100	10.4	10.4
11	23083	13	Electron	61260	100	11.4	11.4
12	23085	13	Electron	60189	100	12.5	12.3
13	23086	13	Electron	60477	100	13.5	13.4
14	23099	13	Electron	60672	100	14.5	14.6
15	23097	13	Electron	61140	100	15.5	15.6
16	23095	13	Electron	61029	100	16.5	16.6
17	23094	13	Electron	60747	100	17.5	17.5
18	23093	13	Electron	60831	100	18.5	18.5
19	23092	13	Electron	60918	100	19.5	19.5
20	23091	13	Electron	60546	100	20.5	20.5
21	23090	13	Electron	60360	100	21.4	21.4
22	23089	13	Electron	60519	100	22.4	22.4
23	23088	13	Electron	60846	100	23.4	23.4
24	23087	13	Electron	60528	100	24.4	24.3

4.2. Data Analysis

4.2.1. Root (An Object-Oriented Data Analysis Framework)

Root [8, 9] is an object-oriented framework designed for solving the data analysis challenges of high-energy physics. Before *root*, data analysis systems like PAW and PIAF, which were written in FORTRAN and having 20 year-old libraries, were used; but they were not powerful enough for analyzing large scale data (10 Terabytes per run) of today's experiments like CMS. Therefore in late 1994, the scientist at CERN started to develop a system to overcome the deficiencies of these previous programs. They used

C++ language and followed the object-oriented analysis and design methodology in developing the new system. In late 1995, they completed the system and its first version started to be used in CERN.

In my analysis, I used a C++ program “plotAllHF.C” which was written in *root* framework. This program analyzed the data and produced the energy histograms of 24 towers.

4.2.2. Peak Fitting

Root makes it possible to fit a histogram with several predefined functions like Gaussian, polynomial, exponential and Landau functions with their parameters. There are two ways to fit a histogram with *root*. One way is to use the fit panel and the other is to use TH1::Fit method.

After getting the energy histograms of all towers, I fit some portion of the histogram to Gaussian function using TH1::fit method by *root*. The Gaussian function is:

$$f(x) = \frac{1}{\sigma\sqrt{2\pi}} \exp\left[-\frac{1}{2}\left(\frac{x-\mu}{\sigma} \right)^2 \right] \qquad (4.1.)$$

where the parameters σ and μ are the standard deviation and the mean of the distribution, respectively. We determine these parameters from the fit.

In my analysis, first I use C++ program “plotlAllHF.C” to analyze beam data and to get the energy histograms of all towers. After getting the histograms of all towers I fit the peak in those histograms to Gaussian function with the TH1::fit method. Some of the fitted histograms are shown in Figure4.1. The rest of the histograms are shown in Appendix B.

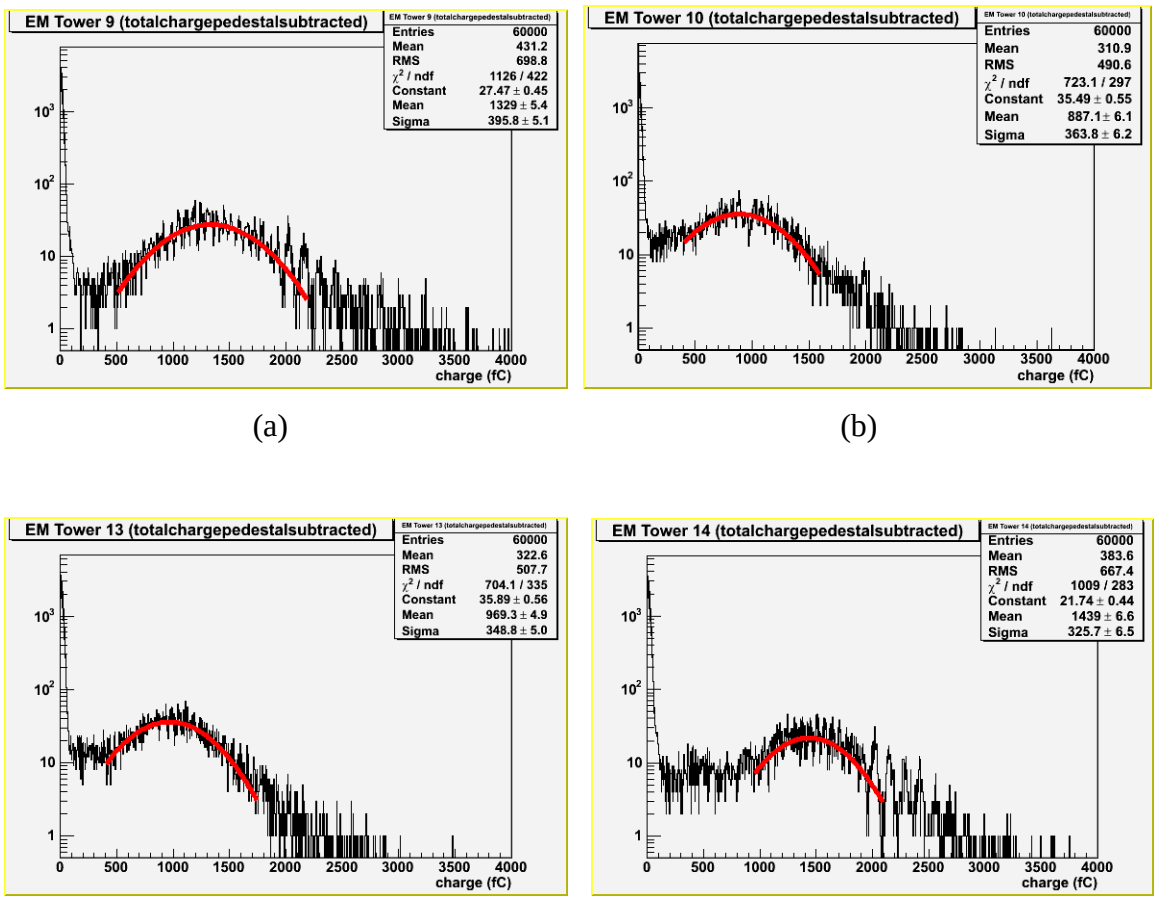

Figure 4.1. The energy histograms of (a) Tower 9, (b) Tower 10, (c) Tower 13 and (d) Tower 14 with Gaussian fit.

4.2.3. Determining the Energy Resolution and the Energy Response

From the fits I obtain the mean and the width (sigma) values of the peaks with their uncertainties. By using the values obtained from the fits I calculate the energy resolution and the energy response of the Towers. To determine the energy response corrected with the PMT gains of the Towers, I used the mean values from the fits and the gain of the PMTs reported in reference [11].

In my analysis, I will also use *Least Squares Method* to fit the energy resolution versus beam energy data to a straight line. In this method, we suppose that the two quantities measured in an experiment are correlated linearly:

$$y_i = a_0 + a_1 x_i \,, \tag{4.2.}$$

where a_0 and a_1 are the parameters to be determined. Hence, the application of the Maximum Likelihood method will result in the simultaneous equations:

$$\sum_k^N (1) \frac{y_k - (a_0 + a_1 x_k)}{\sigma_k^2} = 0 \tag{4.3.}$$

$$\sum_k^N (x_k) \frac{y_k - (a_0 + a_1 x_k)}{\sigma_k^2} = 0 \tag{4.4.}$$

whose solution will yield the best estimates for the parameters a_0 and a_1. Rearranging the expression above yields

$$\sum_k^N \frac{y_k}{\sigma_k^2} = a_0 \sum_k^N \frac{1}{\sigma_k^2} + a_1 \sum_k^N \frac{x_k}{\sigma_k^2} \tag{4.5.}$$

$$\sum_k^N \frac{x_k y_k}{\sigma_k^2} = a_0 \sum_k^N \frac{x_k}{\sigma_k^2} + a_1 \sum_k^N \frac{x_k^2}{\sigma_k^2} \,. \tag{4.6.}$$

The solution of these two simultaneous equations will be

$$a_0 = \frac{1}{D} \left(\sum_k^N \frac{x_k^2}{\sigma_k^2} \sum_k^N \frac{y_k}{\sigma_k^2} - \sum_k^N \frac{x_k}{\sigma_k^2} \sum_k^N \frac{x_k y_k}{\sigma_k^2} \right) \tag{4.7.}$$

and

$$a_1 = \frac{1}{D} \left(\sum_k^N \frac{1}{\sigma_k^2} \sum_k^N \frac{x_k y_k}{\sigma_k^2} - \sum_k^N \frac{x_k}{\sigma_k^2} \sum_k^N \frac{y_k}{\sigma_k^2} \right) \tag{4.8.}$$

where

$$D = \sum_{k}^{N} \frac{1}{\sigma_k^2} \sum_{k}^{N} \frac{x_k^2}{\sigma_k^2} - (\sum_{k}^{N} \frac{x_k}{\sigma_k^2})^2 . \qquad (4.9.)$$

Also we can calculate the uncertainties for the parameters with the following equations;

$$\sigma_{a_0} = \frac{1}{D} \sum_{k}^{N} \frac{x_k^2}{\sigma_k^2} \qquad (4.10)$$

$$\sigma_{a_1} = \frac{1}{D} \sum_{k}^{N} \frac{1}{\sigma_k^2} . \qquad (4.11.)$$

5. RESULTS

5.1. Results as a Function of Tower Number

After obtaining the energy histograms of all Towers, I fit those histograms to a Gaussian function. The mean and sigma values from the fits are used to determine the energy resolutions. Also using the PMT gain values, I determine the corrected energy response values (corrected with the PMT gains). The results are listed in Table 5.1.

From the physical map of HF (Figure 3.6.) we can see that some Towers have the same distance to the beam direction, for example tower 1 and tower 14 have the same distance to the beam direction. So I calculate the weighted average of energy resolution and energy response values of the towers which have the same distance to the beam direction. Figure 5.1 and 5.2 show energy resolution and energy response values versus tower numbers, respectively. For instance in Figure 5.1 energy resolution corresponding to Tower 1 is actually the value of the weighted average of energy resolution values of Tower 1 and Tower 14 which have the same distances to the beam direction. But even though Towers 12 and 13 does not have the same distance, I also calculate the weighted average of their corresponding energy resolution and energy response values.

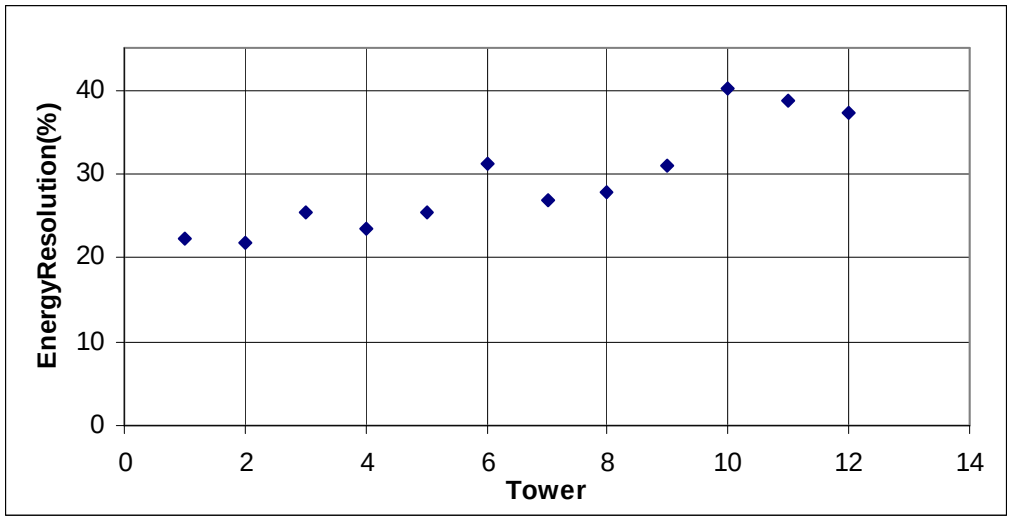

Figure 5.1. Energy resolution versus Tower number.

Table 5.1. Energy resolution and response values for all the towers of wedge 2-13 for 100 GeV electrons.

Tower	Run #	Mean	Sigma	Energy Resolution	Gain	Energy Response (fC)
1	23070	1455±6.2	316.9±6.4	21.8±0.4	15.5±1.6	93.7±9.7
2	23073	1497±7.5	364.8±8.4	24,4±0.6	17.3±1.6	86.8±8.1
3	23075	1461±9.7	403.2±9.9	27.6±0.7	16.6±1.6	88.1±8.5
4	23076	1439±6.6	369.2±7.0	25.7±0.5	15.0±1.6	96.1±10.3
5	23077	1532±6.4	375.4±7.0	24.5±0.5	13.9±1.6	109.9±12.6
6	23078	1179±5.2	365.9±5.4	31.0±0.5	10.5±1.6	112.8±17.3
7	23079	1245±7.0	383.7±7.0	30.8±0.6	12.3±1.6	101.0±13.1
8	23080	1337±6.4	373.6±7.6	27.9±0.6	13.8±1.6	97.1±11.3
9	23081	1329±5.4	395.8±5.1	29.8±0.4	15.1±1.6	88.3±9.4
10	23082	887±6.1	363.8±6.2	41.0±0.8	9.4±1.6	94.3±16.0
11	23083	845±11.6	413.9±11.4	49.0±1.5	9.9±1.6	85.3±13.8
12	23085	1027±11.5	433.2±10.4	42.2±1.1	11.6±1.6	88.9±12.4
13	23086	969±4.9	348.8±5.0	36.0±0.5	9.4±1.6	103.3±17.6
14	23099	1439±6.6	325.7±6.5	22.6±0.5	14.5±1.6	99.6±11.0
15	23097	1617±6.2	325.9±6.9	20.2±0.4	14.9±1.6	108.5±11.6
16	23095	1622±7.8	383.2±10.0	23.6±0.6	15.7±1.6	103.5±10.6
17	23094	1726±6.7	375.9±7.3	21.8±0.4	15.5±1.6	111.4±11.5
18	23093	1439±6.7	380.0±6.5	26.4±0.5	13.1±1.6	109.8±13.4
19	23092	1237±6.4	389.6±6.9	31.5±0.6	10.9±1.6	113.3±16.6
20	23091	1614±6.5	396.8±7.2	24.6±0.5	16.5±1.6	97.7±9.5
21	23090	1343±7.6	374.4±8.7	27.9±0.7	12.5±1.6	107.4±13.7
22	23089	1225±6.2	405.8±6.8	33.1±0.6	10.3±1.6	119.4±18.6
23	23088	1027±7.2	405.7±6.2	39.5±0.7	10.5±1.6	98.2±15.0
24	23087	1086±6.5	398.8±6.7	36.7±0.7	9.7±1.6	112.4±18.6

In figure 5.1 we can see that energy resolution values tend to get poorer with the increasing tower number (decreasing distance to the beam direction). This can be correlated with the PMT gains of towers as we expect to see better energy resolutions with higher gain PMTs. We know that the PMTs are installed in such a way that the PMT

gains of towers increases with the increasing distance to the beam direction. The inner group which consists of towers 10, 11, 12, 13, 23, 24 has low PMT gains. The center group which consists of towers 5, 6, 7, 8, 9, 18, 19, 20, 21, 22 has medium PMT gains. The outer group which consists of towers 1, 2, 3, 4, 14, 15, 16, 17 has high PMT gains.

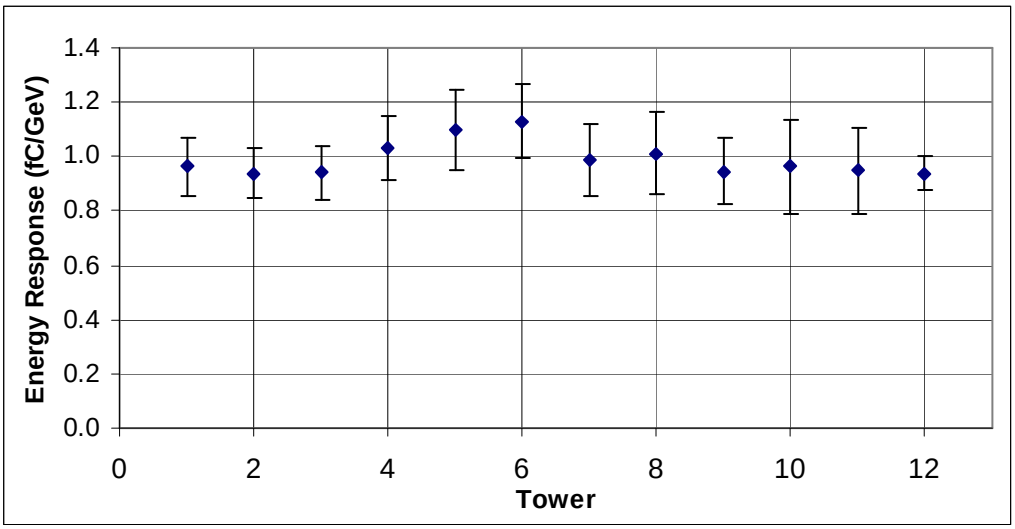

Figure 5.2. Energy response corrected with the PMT gains of towers (peak position /(gain*beam energy)) versus the Tower number.

In Figure 5.2 we can see that there is some significant non-linearity (deviation from the flat response) especially for Tower 5 and Tower 6. The non-linearities for Tower 5 and Tower 6 are 9 per cent and 13 per cent, respectively. But we can see that the overall non-linearity is about 10 per cent.

5.2. Results as a Function of Energy

In addition to analyzing the histograms of all towers I also analyzed the histograms of Tower 2 at four different energies; 30GeV, 50GeV, 100GeV, and 150GeV. The histograms with Gaussian fits are shown in Figure 5.3. The energy resolution and energy response values of the fits are summarized in Table 5.2.

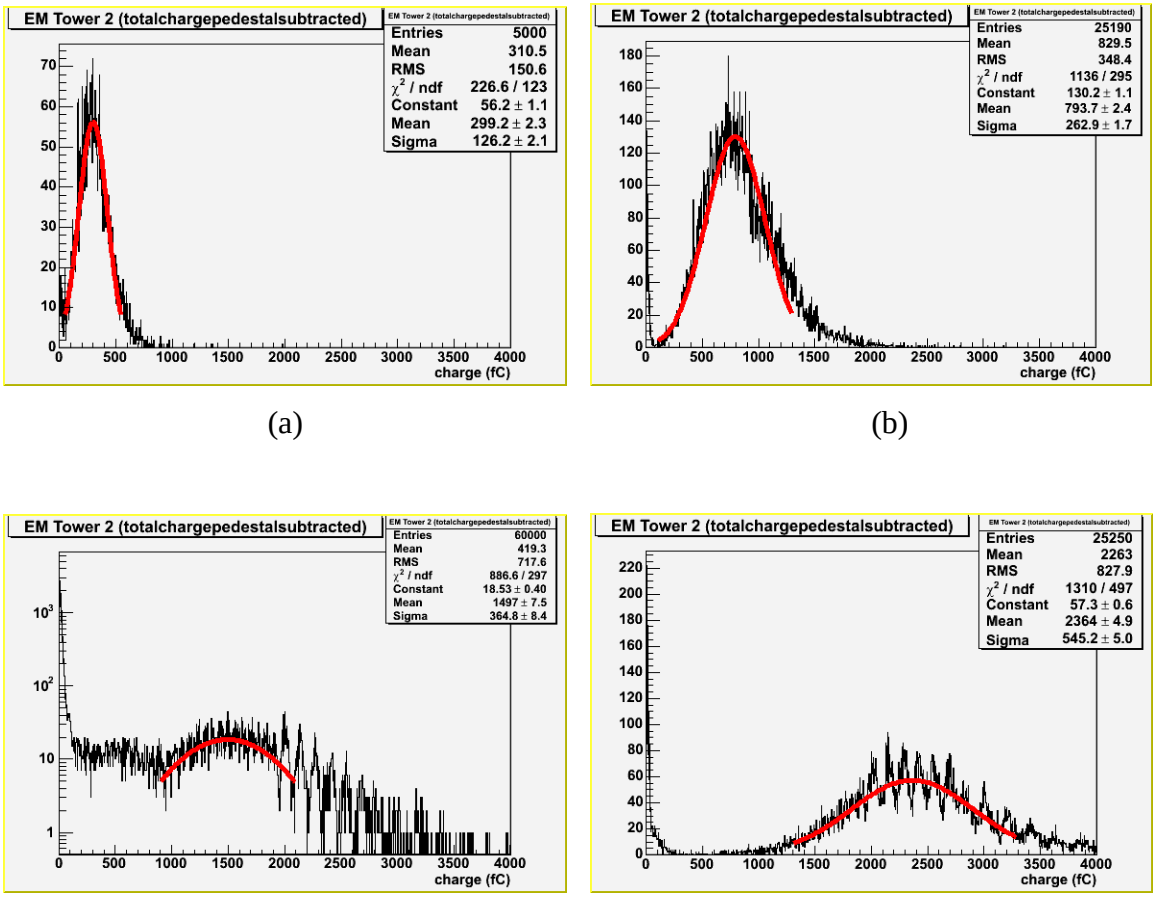

Figure 5.3. Energy histogram for Tower 2 at (a) 30 GeV, (b) 50GeV, (c) 100GeV, (d) 150GeV.

Table 5.2. Energy resolution and response values as a function of electron beam energy for Tower 2 (wedge 2-13).

Tower	Energy (GeV)	Run #	Mean	Sigma	Energy Resolution	Gain	Energy Response (fC)
2	30	22849	299.2±4.9	126.2±2.1	42.2±1.0	17.3±1.6	17.3±1.6
2	50	22447	793.7±7.5	262.9±1.7	33.1±0.4	17.3±1.6	45.9±4.3
2	100	23073	1497.0±2,4	364.8±8.4	24.4±0.6	17.3±1.6	86.5±8.1
2	150	22479	2364.0±2.3	545.2±5.0	23.1±0.2	17.3±1.6	136.6±12.7

Using the data listed in Table 5.2, I plot the energy resolution versus $1/\sqrt{E}$ values in Figure 5.4. Also in Figure 5.5 we can see the plot of the corrected energy response versus energy values. Fitting the data in Figure 5.4 to a straight line;

$$y = a_0 + a_1 x \tag{5.1.}$$

yields the following results:

$$a_0 = 15.01 \pm 0.05 \tag{5.2a.}$$

$$a_1 = 158.7 \pm 5.28 \tag{5.2b.}$$

where the unit of a_1 is GeV$^{-1/2}$.

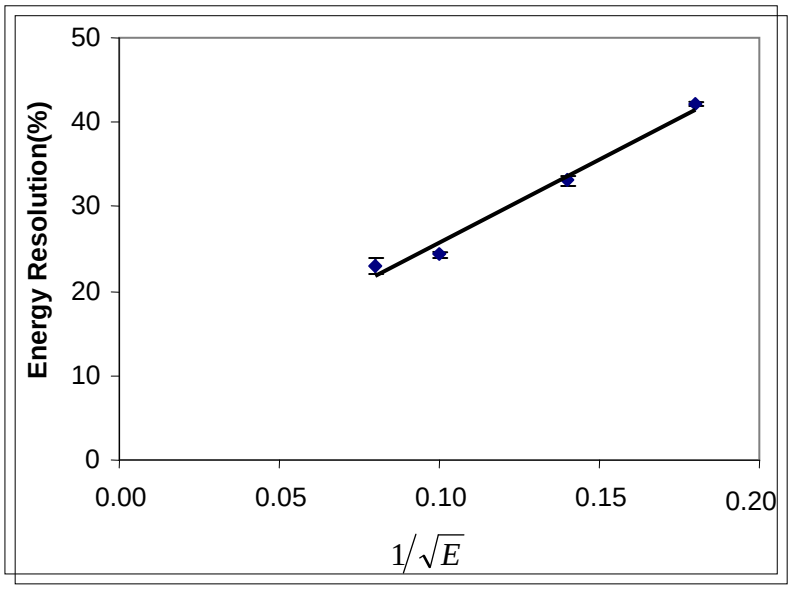

Figure 5.4. Energy resolutions versus $1/\sqrt{E}$.

In Figure 5.5 we can see that the energy response as a function of beam energy is flat about 0.9 except for 30GeV data. The test beam run used for 30GeV analysis has very low statistics compared to the other runs.

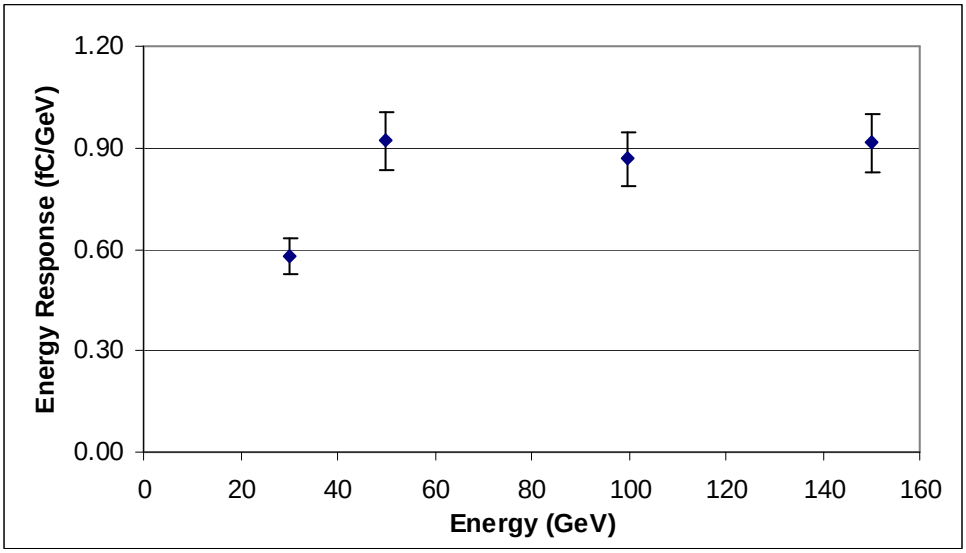

Figure 5.5. Energy response corrected with the PMT gains (peak position/(gain*beam energy)) as a function of beam energy.

6. CONCLUSION

In this work, I studied the energy resolution and the energy response of the HF Forward Calorimeter for electrons as functions of tower number and beam energy using the test beam data for wedge 2-13 taken during the HF Test Beam 2004 period.

If we calculate the average energy resolution of the groups (inner, center and outer), we can see that the energy resolution gets worse with the decreasing PMT gain values as seen in Table 6.1. This is expected since low PMT gain means low statistics in the number of electrons collected at the anode thereby yielding poor resolution.

Table 6.1. Energy resolution of the PMT Groups

Groups	Average Gains	Average Energy Resolution
Inner	14.4	38.7
Center	15.6	28.5
Outer	16.3	22.9

In Figure 5.4. we see the energy resolution for electrons as a function of energy. Fitting the energy resolution versus $1/\sqrt{E}$ to a straight line results in $a_0 = 15.01 \pm 0.05$ and $a_1 = 158.7 \pm 5.28$. We know that these values give us the following equation,

$$(\sigma/E)_{tot} = 15.01\% + \frac{158.7\%}{\sqrt{E}}. \qquad (6.1)$$

In this equation the first term at r.h.s. is energy independent and sets the limit for the performance at very high energies (15 per cent). The second term is energy dependent and determines the performance over much of the useful range of the calorimeter.

To conclude, the results for the energy resolution are as expected for the HF Forward Calorimeter which is a Quartz Fiber Calorimeter. But the same is not true for the energy response results; there are some non-linearities. Energy response requires more detailed analysis.

APPENDIX A: PLOTALLHF.C

```
#include <HFTowers.hh>
void plotALLHF() {
  printf("\n\n");
  printf("Usage:\n");
  printf("------\n\n");
  printf("plotALLHF(   (int) run number,\n");
  printf("  (optional) (char) tower type,\n");
  printf("  (optional) (int) number of events )\n");
  printf("\n");
  printf("Examples:\n");
  printf("---------\n");
  printf("plotALLHF( 13282 )\n");
  printf("plotALLHF( 13283, \"em\", 1000 )\n");
  printf("\n");
  printf("Defaults:\n");
  printf("---------\n");
  printf("tower type       ---> em\n");
  printf("number of events ---> 1000\n");
  printf("\n");
  printf("Notes:\n");
  printf("------\n");
  printf("The available tower types are: \"em\" and \"ha\".\n");
  printf("\n");
}

void plotALLHF(int runNumber, TString towerType="em", int maxEvents=1000,
bool makePlot=true) {

  int EM_HA = 999;
```

```
towerType.ToLower();
if( !strcmp(towerType.Data(), "em") ) {
 EM_HA = _EM_;
}
else if( !strcmp(towerType.Data(), "ha") ) {
 EM_HA = _HA_;
}
else {
 cout << "Tower type not specified correctly: " << towerType.Data() << endl <<
endl;
 return;
}

gDirectory->DeleteAll();
gROOT->LoadMacro("basics.cc");

towerType.ToUpper();

TH1F *pulses[_TOWERS_];
TH1F *tpulses[_TOWERS_];
TH1F *totalEnergy;
TH2F *totPulses, *mTiming;
for( int i = 0; i < _TOWERS_; i++ ) {
 char s[50];
 sprintf(s,"%s Tower %d pedestal subtracted",towerType.Data(),i+1);
 pulses[i] = new TH1F( s, s, 20, -0.5, 19.5 );
 pulses[i]->GetXaxis()->SetTitle("time slice");
 sprintf(s,"%s Tower %d total charge pedestal subtracted",towerType.Data(),i+1);
 tpulses[i] = new TH1F( s, s, 2500, 0, 2500 );
 tpulses[i]->GetXaxis()->SetTitle("charge (fC)");
}
sprintf(s,"%s HF Total Pulses Map",towerType.Data());
```

```
  totPulses = new TH2F( s, s, 2, 0, 2, 13, 1, 14 );
  sprintf(s,"%s HF Mean Timing Map",towerType.Data());
  mTiming = new TH2F( s, s, 2, 0, 2, 13, 1, 14 );
  sprintf(s,"%s HF Total Energy", towerType.Data());
  totalEnergy = new TH1F( s, s, 25000, 0, 25000 );

  DCCData* dcc;
  HFTowers *hf = new HFTowers();

  unsigned short buffer[25];
  double data[20];
  char fiber, qieid, er, dv, cap, qie;
  float highest_energy=0.;

  char filename[200];
//  sprintf(filename,"/outdata/HTB_%06d.root",runNumber);
  sprintf(filename,"/home/canko/scratch0/HF/HTB_%06d.root",runNumber);
  if( gSystem->AccessPathName(filename) ) {
    cout << endl << "File: " << filename << " not there!!!" << endl << endl;
    return;
  }
  else ;
  TestBeamDataFile f;
  f.load(filename);

  double totEvents = f.getNEvents();
  int nEvents = 0;
  int goodEvents = 0;
  int badCaps = 0;
  int hardInfo[2] = {999,999};

  while( f.getNextEvent() && nEvents++ < maxEvents ) {
```

```
 dcc = f.getEventData()->getHCALData()->getDCC(_DCC_);

 float tenergy=0.;
 for(int ntower = 1; ntower <= _TOWERS_; ntower++) {

  float eenergy=0.;

  hf->decode2hardware( EM_HA, ntower, hardInfo );
  dcc->getQIEData( hardInfo[0], hardInfo[1], buffer );

  // check caps (function in basics.cc) //
  bool capok = isCapOK( buffer );
  float pedestal = estimatePedestal( dcc, buffer );
  bool hasAP = false;

  if( capok ) {
for(int tslice = 0; tslice < 20; tslice++) {
 DCCData::parseQIE(buffer[tslice],fiber,qieid, er, dv, cap, qie);
 data[tslice] = dcc->convertToFC_noninv(qie)-pedestal;

 pulses[ntower-1]->Fill( tslice, data[tslice] );
 eenergy += data[tslice];
 goodEvents++;
}
tpulses[ntower-1]->Fill( eenergy );
tenergy += eenergy;
  }
  else {
badCaps++;
  }
 }
```

```
  if( tenergy > highest_energy ) {
   highest_energy = tenergy;
  }
  else ;
  totalEnergy->Fill( tenergy );
 }
 goodEvents /= (20*24); // <--- divide by number of channels and time slices
 cout << "Processed " << nEvents << " events and " << goodEvents << " good
events." << endl;
 cout << "There were " << badCaps << " bad caps." << endl;
 f.close();

 float gtheTowers[_TOWERS_];
 float gttiming[_TOWERS_], gttimRMS[_TOWERS_];
 float gmeans[_TOWERS_], gmeansRMS[_TOWERS_];

 for( int aps = 0; aps < _TOWERS_; aps++ ) {
  if( pulses[aps]->GetEntries() )
   pulses[aps]->Scale( 20./pulses[aps]->GetEntries() );
  else ;

  if( aps+1 < 12 ) {
   totPulses->Fill( 0, aps+1, pulses[aps]->Integral() );
   mTiming  ->Fill( 0, aps+1, pulses[aps]->GetMean() );
  }
  else if( aps+1 > 13 ) {
   totPulses->Fill( 1, (aps+1)-13, pulses[aps]->Integral() );
   mTiming  ->Fill( 1, (aps+1)-13, pulses[aps]->GetMean() );
  }
  else if( aps+1 == 12 || aps+1 == 13 ) {
   totPulses->Fill( 0, aps+1, pulses[aps]->Integral() );
   totPulses->Fill( 1, aps+1, pulses[aps]->Integral() );
```

```
   mTiming  ->Fill( 0, aps+1, pulses[aps]->GetMean() );
   mTiming  ->Fill( 1, aps+1, pulses[aps]->GetMean() );
  }
  else ;
  gtheTowers[aps] = aps+1;
  gttiming[aps]   = pulses[aps]->GetMean();
  gttimRMS[aps]   = pulses[aps]->GetRMS();
  gmeans[aps]     = tpulses[aps]->GetMean();
  gmeansRMS[aps]  = tpulses[aps]->GetRMS();
}

TGraph *gr_means = new TGraph( _TOWERS_, gtheTowers, gmeans );
gr_means->SetTitle("mean of pulses");
gr_means->SetMarkerStyle(20); gr_means->SetMarkerSize(1);
TGraph *gr_meRMS = new TGraph( _TOWERS_, gtheTowers, gmeansRMS );
gr_meRMS->SetTitle("RMS of pulses");
gr_meRMS->SetMarkerStyle(20); gr_meRMS->SetMarkerSize(1);
TGraph *gr_timing = new TGraph( _TOWERS_, gtheTowers, gttiming );
gr_timing->SetTitle("mean of timing");
gr_timing->SetMarkerStyle(20); gr_timing->SetMarkerSize(1);
TGraph *gr_timRMS = new TGraph( _TOWERS_, gtheTowers, gttimRMS );
gr_timRMS->SetTitle("RMS of timing");
gr_timRMS->SetMarkerStyle(20); gr_timRMS->SetMarkerSize(1);

if( makePlot ) {
  TCanvas* c1 = new TCanvas("c1","Channels 1-6");
  c1->Divide(2,3);
  for (int i=0; i<6; i++) {
    c1->cd(i+1); pulses[i]->Draw();
  }
  TCanvas* c2 = new TCanvas("c2","Channels 7-12");
  c2->Divide(2,3);
```

```
for (int i=0; i<6; i++) {
  c2->cd(i+1); pulses[i+6]->Draw();
}
TCanvas* c3 = new TCanvas("c3","Channels 13-18");
c3->Divide(2,3);
for (int i=0; i<6; i++) {
  c3->cd(i+1); pulses[i+12]->Draw();
}
TCanvas* c4 = new TCanvas("c4","Channels 19-24");
c4->Divide(2,3);
for (int i=0; i<6; i++) {
  c4->cd(i+1); pulses[i+18]->Draw();
}
TCanvas* c11 = new TCanvas("c11","Channels 1-6");
c11->Divide(2,3);
for (int i=0; i<6; i++) {
  c11->cd(i+1); tpulses[i]->Draw();
}
TCanvas* c12 = new TCanvas("c12","Channels 7-12");
c12->Divide(2,3);
for (int i=0; i<6; i++) {
  c12->cd(i+1); tpulses[i+6]->Draw();
}
TCanvas* c13 = new TCanvas("c13","Channels 13-18");
c13->Divide(2,3);
for (int i=0; i<6; i++) {
  c13->cd(i+1); tpulses[i+12]->Draw();
}
TCanvas* c14 = new TCanvas("c14","Channels 19-24");
c14->Divide(2,3);
for (int i=0; i<6; i++) {
  c14->cd(i+1); tpulses[i+18]->Draw();
```

```
}

TCanvas *cE = new TCanvas("cE","Total Energy");
totalEnergy->GetXaxis()->SetRangeUser( 0, 1.1*highest_energy );
totalEnergy->Draw();

TCanvas *cMeans = new TCanvas("cMeans","Tower Mean/RMS");
cMeans->Divide(1,2);
cMeans->cd(1);
gr_means->Draw("ap");
cMeans->cd(2);
gr_meRMS->Draw("ap");

TCanvas *cTiming = new TCanvas("cTiming","Timing Mean/RMS");
cTiming->Divide(1,2);
cTiming->cd(1);
gr_timing->Draw("ap");
cTiming->cd(2);
gr_timRMS->Draw("ap");

TLatex *binLabels = new TLatex();
float x, y;
char ltext[5];

gStyle->SetPalette(1);
TCanvas *cT = new TCanvas("cT","Mean Timing");
cT->SetFillColor(0);
mTiming->SetAxisColor(0,"X");  mTiming->SetAxisColor(0,"Y");
mTiming->SetTickLength(0,"X"); mTiming->SetTickLength(0,"Y");
mTiming->SetLabelSize(0,"X");  mTiming->SetLabelSize(0,"Y");
mTiming->SetAxisRange(0.,20.,"Z");
mTiming->Draw("colz");
```

```
 mTiming->SetStats(kFALSE);
 for( int i = 0; i < _TOWERS_; i++ ) {
  if( i+1 < 12 ) {
x = 0.5;
  }
  else if( i+1 == 12 || i+1 == 13 ) {
x = 1.;
  }
  else {
x = 1.5;
  }
  if( i+1 == 1 || i+1 == 14 ) {
y = 1.3;
  }
  else {
y += 1.;
  }
  sprintf(ltext,"%d",i+1);
  binLabels->DrawLatex(x,y,ltext);
 }

 TCanvas *cP = new TCanvas("cP","Total Pulses");
 cP->SetFillColor(0);
 totPulses->SetAxisColor(0,"X");  totPulses->SetAxisColor(0,"Y");
 totPulses->SetTickLength(0,"X"); totPulses->SetTickLength(0,"Y");
 totPulses->SetLabelSize(0,"X");  totPulses->SetLabelSize(0,"Y");
 totPulses->Draw("colz");
 totPulses->SetStats(kFALSE);
 for( int i = 0; i < _TOWERS_; i++ ) {
  if( i+1 < 12 ) {
x = 0.5;
  }
```

```
    else if( i+1 == 12 || i+1 == 13 ) {
  x = 1.;
    }
    else {
  x = 1.5;
    }
    if( i+1 == 1 || i+1 == 14 ) {
  y = 1.3;
    }
    else {
  y += 1.;
    }
    sprintf(ltext,"%2d",i+1);
    binLabels->DrawLatex(x,y,ltext);
   }

  }
  else {
   cout << "LOOK HERE" << endl;
   for( int i = 0; i < _TOWERS_; i++ ) {
    cout << pulses[i]->Integral() << "   ";
   }
   cout << endl;
  }

}
```

APPENDIX B: ALL HISTOGRAMS

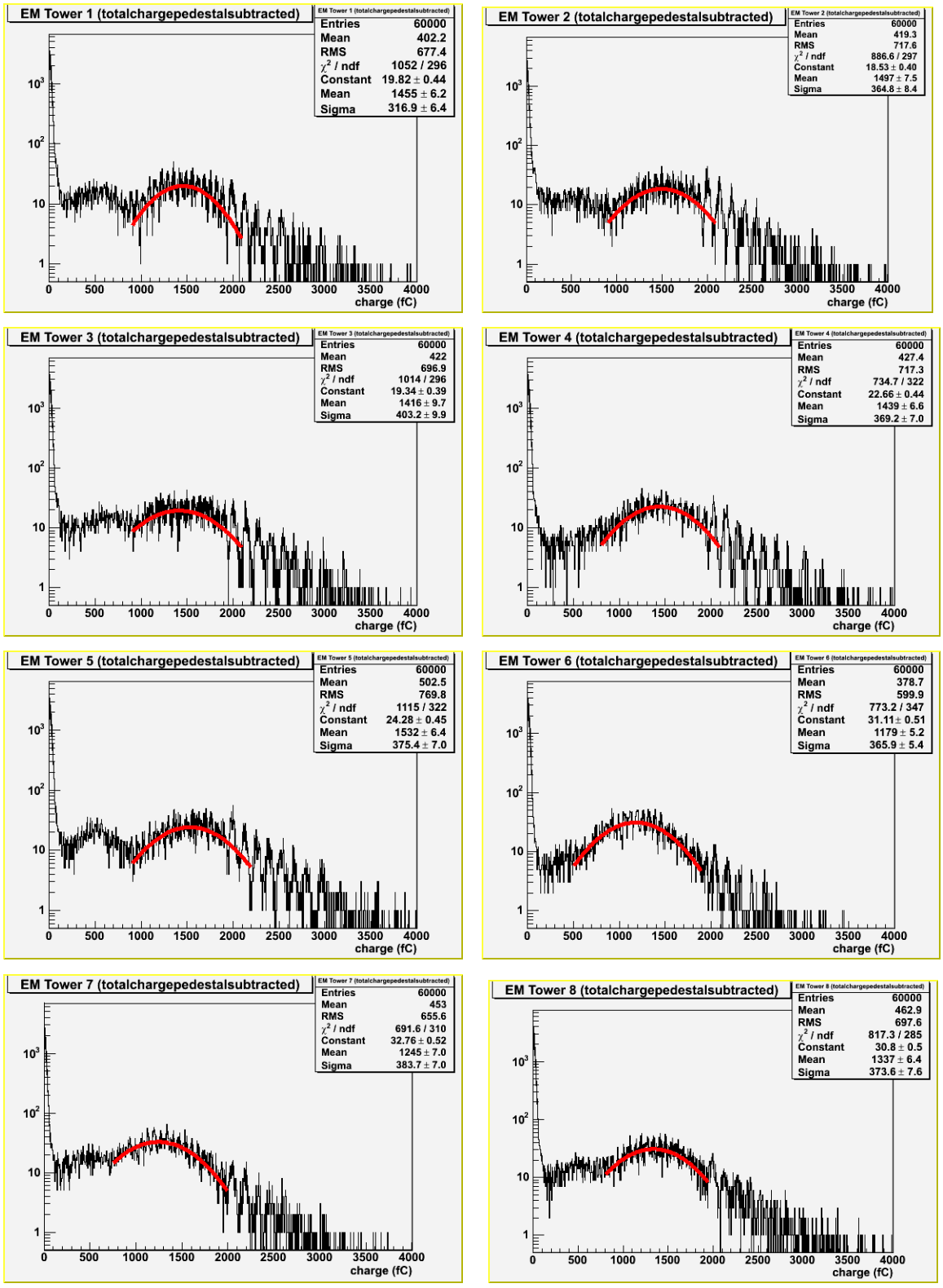

Figure B.1. The energy histograms of all towers with Gaussian fit (cont').

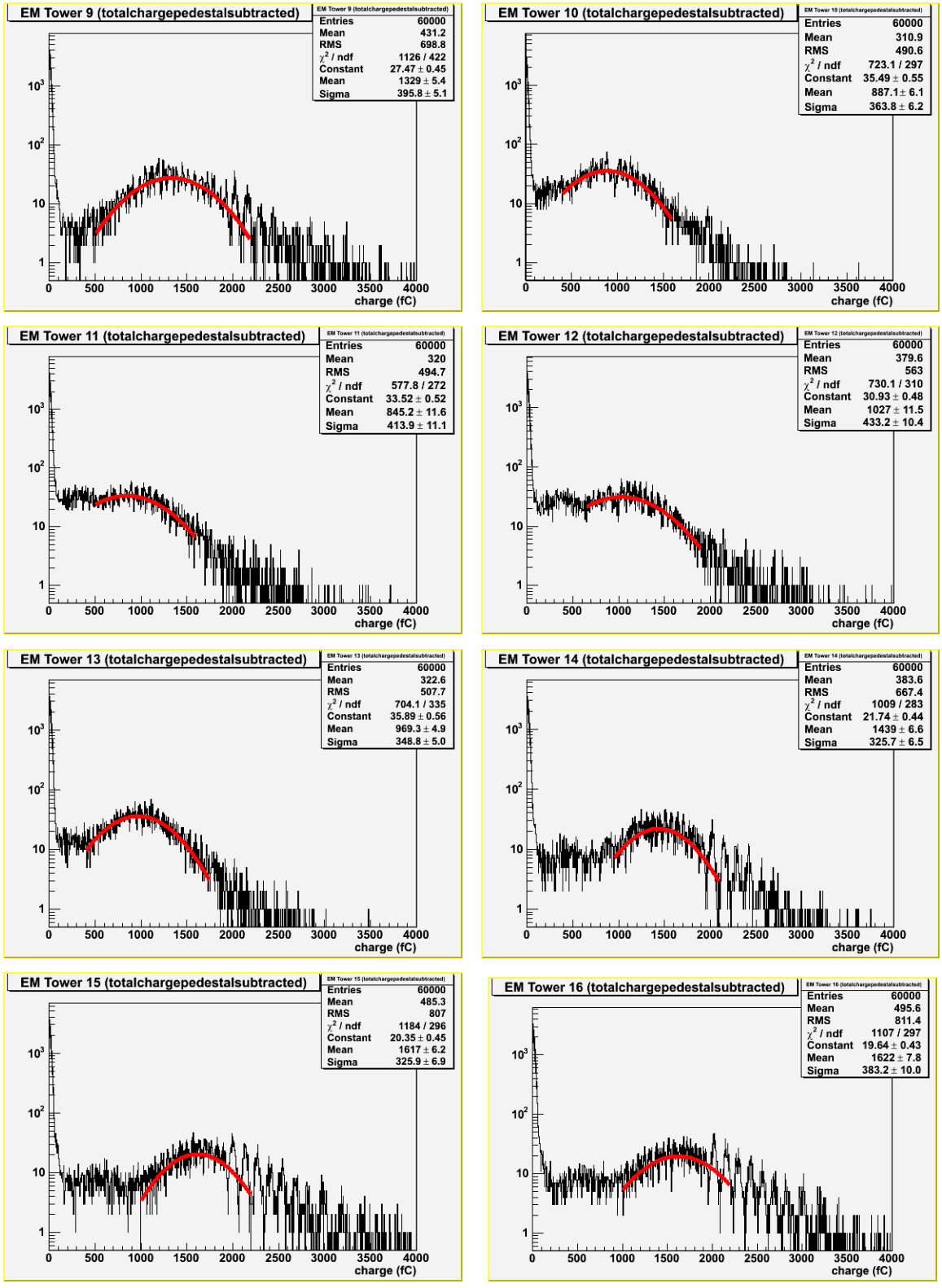

Figure B.1. The energy histograms of all towers with Gaussian fit (cont').

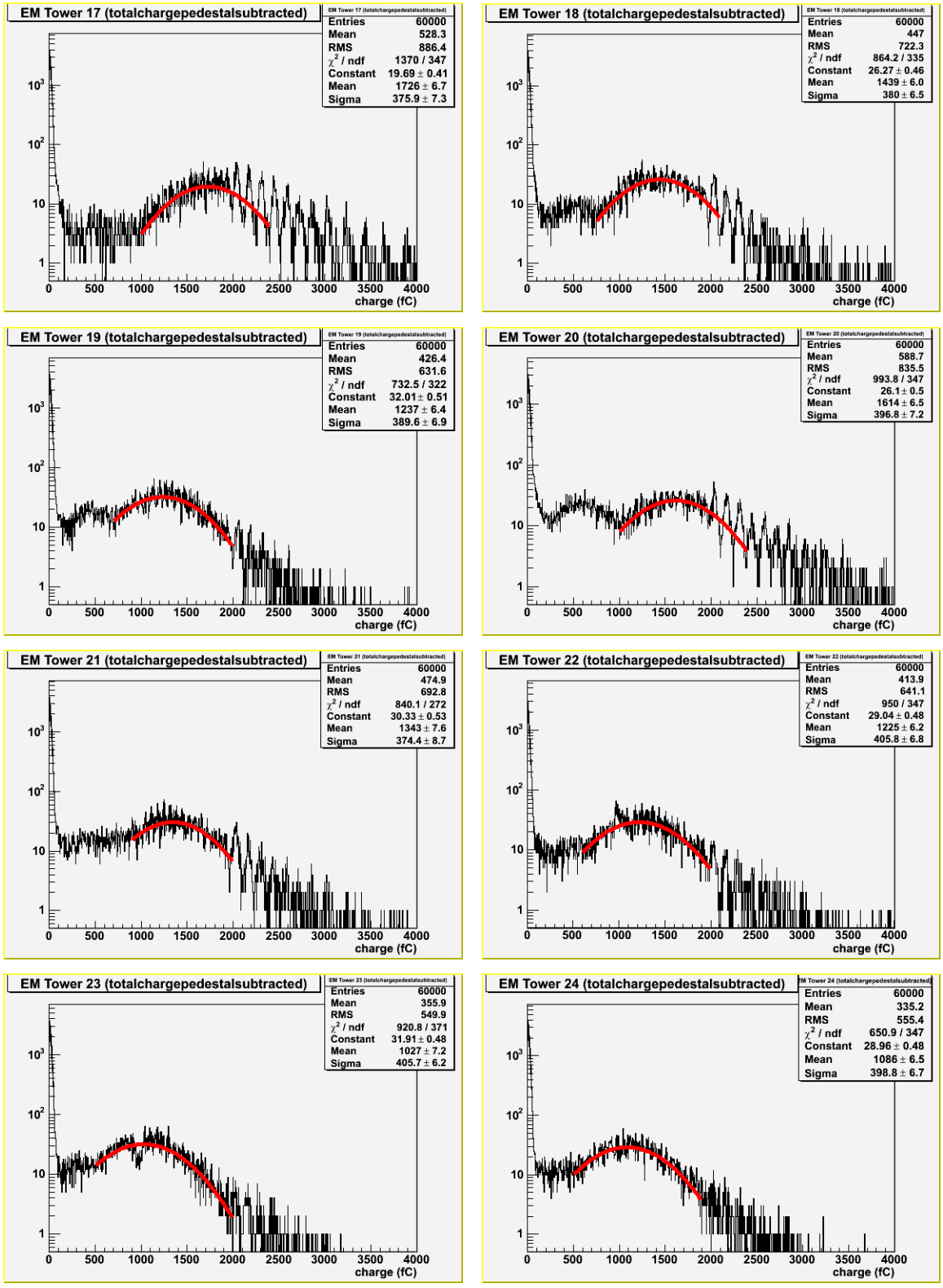

Figure B.1. The energy histograms of all towers with Gaussian fit (cont').

REFERENCES

1. Martin, B.R. and Shaw G., *Particle Physics*, John Willey & Sons, 1997.

2. Ferbel, T., *Experimental Techniques in HEP*, Addison-Wesley, 1987.

3. Green D., *The Physics of Particle Detectors*, Cambridge University Press, 2000.

4. Hughes, I.S., *Elementary Particles*, Cambridge University Press, 1991.

5. Wigmans, R., *Calorimetry*, Oxford University Press New York, 2000.

6. http://cms.info.cern.ch/2005.

7. *HCAL Technical Design Report*, CERN, June 1997.

8. http://root.cern.ch, 2005.

9. Brun, R. et al., *The ROOT Users Guide*, CERN, ftp://root.cern.ch/ User_Guide_4.08.pdf, July 2004.

10. Gülmez E., *Basic Data Analysis for Experiments in the Physical Sciences*, Boğazici University Printhouse, Istanbul, 1997.

11. Dindar K., *Comparison of relative PMT gains measured at the University of Iowa and those obtained from source run data taken during the HF Test Beam 2004 period*, M. S. Thesis, Bogazici University, June 2005.